



Exergetic and economic optimization of a solar-based cogeneration system applicable for desalination and power production

Ramin Ghasemiasl¹ · Mohammad Amin Javadi¹ · Morteza Nezamabadi² · Mohsen Sharifpur^{3,4}

Received: 11 June 2020 / Accepted: 12 September 2020 / Published online: 9 October 2020
© Akadémiai Kiadó, Budapest, Hungary 2020

Abstract

In this research, the optimum situation for the function of a combined cycle power plant (CCPP) which simultaneously generates water and electricity with parabolic solar collectors has been scrutinized. The CCPP includes two gas cycles and one steam cycle in which a multi-stage vapor desalination and a parabolic solar collector have been added. In this stage, first, the thermodynamic cycle of the CCPP has been modeled, and values of exergy and energy in each flow line and the power plant component were determined. Finally, exergy destruction in each section is calculated. For a better assessment of the system, an economic analysis of power plant is performed by using SPECO method. The results revealed that as the number of desalination effect increased from 4 to 8 and the exergy efficiency decreased from 52.7 to 52.4%. Moreover, there was an increase in the cost of electricity generation by 12%, and the interest rate of freshwater production increased from 6 to 12 due to the increase in the number of effects. The power plant optimization results show that the exergy efficiency increases to 53.62%, which indicates a growth of 1.74%.

Keywords Combined cycle · Cogeneration power plant · Desalination · Exergy destruction · Environmental effect · Exergy efficiency · Solar collector

List of symbols

c	Cost per exergy unit (\$ (MJ) ⁻¹)
c_f	Cost of fuel per energy unit (\$ (MJ) ⁻¹)
\dot{C}	Cost flow rate (\$ s ⁻¹)
c_p	Specific heat at constant pressure (kJ kg ⁻¹ K ⁻¹)
CRF	Capital recovery factor
\dot{E}_x	Exergy flow rate (MW)
$\dot{E}_{x,D}$	Exergy destruction rate (MW)
ex	Specific exergy (kJ kg ⁻¹)
i	Annual interest rate (%)

h	Specific enthalpy (kJ kg ⁻¹)
h_0	Specific enthalpy at environmental state (kJ kg ⁻¹)
LHV	Lower heating value (kJ kg ⁻¹)
\dot{m}	Mass flow rate (kg s ⁻¹)
n	Number of years
N	Number of hours of plant operation per year
PP	Pinch point
\dot{Q}	Heat transfer rate (kW)
r_{AC}	Compressor pressure ratio
s	Specific entropy (kJ kg ⁻¹ K ⁻¹)
s_0	Specific entropy at environmental state (kJ kg ⁻¹ K ⁻¹)
\dot{W}_{net}	Net power output (MW)
Z	Capital cost of a component (\$)
\dot{Z}	Capital cost rate (\$ s ⁻¹)

✉ Mohammad Amin Javadi
Benyaminjava@gmail.com

✉ Mohsen Sharifpur
mohsen.sharifpur@up.ac.za;
mohsensharifpur@duytan.edu.vn

¹ Department of Mechanical Engineering, West Tehran Branch, Islamic Azad University, Tehran, Iran

² Department of Mechanical Engineering, Iran University of Science and Technology, Tehran, Iran

³ Department of Mechanical and Aeronautical Engineering, University of Pretoria, Pretoria, South Africa

⁴ Institute of Research and Development, Duy Tan University, Da Nang 550000, Vietnam

Greek letters

η	Isentropic efficiency
ξ	Coefficient of fuel chemical exergy
Φ	Maintenance factor

Subscripts

a	Air
AC	Air compressor
CC	Combustion chamber

CCPP	Combined cycle power plant
ch	Chemical
Cond	Condenser
COE	Cost of electricity
GT	Gas turbine
HP	High pressure
HRSG	Heat recovery steam generator
IAM	Incidence angle modifier
LP	Low pressure
MED	Multi-effect distillation
MSF	Multi-stage flash
ph	Physical
ST	Steam turbine
SWRO	Sea water reverse osmosis
TVC	Thermal vapor compression
w	Water

Introduction

Using simultaneous production systems which are not either applied for generating electricity but also for desalination could help to overcome the issues related to heat loss which might lead to a decrease in the thermal efficiency of power plants. Cogeneration technologies could be considered as an effective method since they use thermal recovery instead of an independent energy source for producing products.

There are many types of research on the multi-generation systems with power production and desalination units. Among them, Hornburg et al. [1] and El-Nashar et al. [2] are from the most important ones. In these researches, steam turbine and gas turbine are considered to generate electricity beside RO & MSF for desalination.

Kronenberg et al. [3] investigated a multi-generation system using two low-temperature sources (one diesel power plant and one steam power plant) for a low-temperature MED system.

An exergy-economic analysis was done on a 500 MW CCPP by Javadi et al. [4]. The results showed the highest exergy destruction level occurs in the combustion chamber. Also, increasing the condenser pressure reduces the exergy efficiency by 2%.

The electricity costs were calculated by Rensonnet et al. [5] for various combinations of RO, MED and RO/MED hybrid system with a gas turbine power plant. The results revealed that the exergy costs for water production through RO are far less than MED system. Considering for cost reduction in the water production sector as the objective helped them to approach this goal but increased the overall costs of the system; therefore, for optimizing the whole system, reduction in the overall costs was considered as a goal.

Complete research took place by Mahbub et al. [6] for economic investigation of various combinations of a

simultaneous production system including CCPP with RO, MSF, MED, MSF/RO and MED/RO. As a result, the combination of CCPP with MED/RO revealed the least fuel consumption, especially compared to the conventional-combined cycle integrated with MSF/RO.

In research done by He et al. [7], a mechanical vapor compression desalination system was investigated in interaction with a transcritical carbon dioxide Rankine cycle. In this cycle, the boiler was used for water evaporation. After that, the evaporated water passes over the Rankine cycle and providing the demanded power enters the converter of vapor compression system. The steam will be extracted in the separator and will be compressed through the produced work in the Rankine cycle, and then it would be distilled. The results of the thermodynamic analysis showed that the combination of these two systems has high reliability and performance. Moreover, these results confirmed the ability of water production with 1.29 kg s^{-1} mass flow rate in this cycle.

Due to the availability and wide ranges of applicability of solar energy [8], it can be used in different multi-generation systems. In a research done by Habibollahzade et al. [9], an energy system including parabolic solar collectors (PTSC), thermoelectric generator (TEG), Rankine cycle and a proton exchange membrane fuel cell (PEM) were optimized. The optimization process was done by employing a multi-objective genetic algorithm. The results coming out from this optimization showed that the exergy efficiency increased from 12.76 to 13.29%.

An exergy-economic analysis was done on a combined solar-waste-driven power plant by Sadi et al. [10]. The electricity production cost in the studied power plant was $0.202 \text{ \$ (MJ)}^{-1}$. The proposed solutions for the modification of the power plant resulted in $0.137 \text{ \$ (MJ)}^{-1}$ reduction in the cost of produced electricity.

Energy, exergy, exergoeconomic and environmental (4E) analysis of a cooling, heating and power production of a CCPP was addressed by Wang et al. [11]. Solar energy has been used by a parabolic solar collector. The results showed that energy and exergy efficiency was 83.6% and 24.9% in cooling mode and 66% and 25.7% in the heating mode, respectively. The ratio of carbon emission reduction in the combined energy production system unit was approximately 41% in comparison with a system without solar energy.

A multi-generation system consisting of a multi-stage evaporative desalination and a power production Rankine cycle was investigated by Ortega-Delgado et al. [12]. The demanded energy for the cycle was provided by centralized solar energy system with parabolic collectors. In order to make the possibility of change in parameters and achieve the best results, ejector nozzles with variable opening were used to maintain the flexibility of the desalination system in different operating conditions.

A combination of a MED desalination system with a supercritical CO₂ gas power plant was investigated by Sharan et al. [13]. This study considered a multi-generation system in San Diego that includes a power plant with a capacity of 115 MW with 48% efficiency and a capacity factor of 46.9% (in which the supercritical CO₂ leaves the cycle in 71.5 °C and was used for MED system.) and also a MED system with production capacity of 1558 m³ desalinated water (which costs 1.81 dollar per cubic meters) per day as the reference cycle. After performance modeling, the system was investigated for various locations, and the results showed that among all the cases, Saudi Arabia has the lowest cost for simultaneous production of water and electricity.

A multi-generation system was evaluated by Yilmaz et al. [14]. The system was used for simultaneous generation of electricity and hydrogen, cooling, heating and water desalination by using solar Heliostat, Brayton Cycle, Organic Rankine Cycle, absorption heating and cooling system, MSF desalination system and a PEM electrolyzer unit. Different parameters such as the inlet pressure of turbine, solar radiation, isentropic efficiency of compressor and temperatures were analyzed. The results showed that energy and exergy efficiencies of the system were 79% and 49%, respectively, which was obtained for water and hydrogen mass flow rates of 886 and 47 g s⁻¹.

A cogeneration system includes multi-effect desalination and organic Rankine cycle was simulated by Ghorbani et al. [15]. The proposed system was utilized for producing fresh water and power. The results show that efficiency of the organic Rankine cycle power plant and GOR of the MED system is 12.47% and 2.918, respectively.

In another research done by Demir et al. [16], a combined system for power generation and water desalination was analyzed. This system consisted of three main parts: A hybrid system used for providing thermal energy that works by solar energy, a thermoelectric generator system (TEG) and a Rankine cycle. The main heat source in this research was a solar-powered compressed air. In this system, natural gas system was used as the alternative for the cases solar radiation was less than 900 W/m². In addition, thermoelectric was applied for generating electricity through gas turbine waste heat. This system was capable of producing 21.8 MW electricity and 3.36 kg s⁻¹ desalination capacity.

A multi-generation system including gas turbine power cycle with a solar parabolic collector, a steam turbine, HRSG, MED and absorption chiller has been proposed by Ansari et al. [17]. The proposed model was optimized by GA method. Optimization of this multi-generation system has resulted in an optimal design point of exergy efficiency of 36.16% and a total cost rate of 188.43 \$/h.

In energy systems, exergy analysis is an important tool due to the significance of the origin and amount of energy destruction during processes. Despite the high importance

of exergy analysis, there were few studies about cogeneration systems based on exergy analysis; therefore, exergy-economic analysis of cogeneration systems is really valuable for better assessment of the existing power plants and the future projects. In the current research, the following goals have been pursued:

- The proposed thermal cycle is modeled based on the exergy-economic analysis
- The results obtained from the code are validated with experimental data from the operation of the power plant.
- The objective function, decision variables and design constraints are defined.
- The system design parameters are optimized by a multi-objective genetic algorithm optimization approach.
- Sensitivity analysis has been performed for the proposed thermal system.

Theory and modeling

In this research, a cogeneration system consisting of gas and steam turbines, a MED system and a solar farm with parabolic collectors is considered. Validation of the combined cycle thermodynamic modeling was compared with the actual data obtained from Abadan CCPP in Iran. In addition, the vapor compression desalination system is compared with the results came from modeling of Al-Mutaz et al. [18] research. The schematic of the proposed thermal cycle is shown in Fig. 1.

In analyzing this configuration, the following assumptions have been considered:

- Turbines, compressors, pumps and condensers are considered adiabatic.
- All processes in this simulation are uniform.
- Kinetic and potential energies are considered negligible.
- Air and combustion gases are assumed as ideal gases.

Exergy-economic analysis is related to the costs of the exergy of each of flow streams. To perform exergy-economic analysis, the exergy rate related to each of input and output lines should be specified.

Combined cycle power plant

The CCPP consists of two gas turbines, two dual-pressure heat recovery steam generator and one steam turbine. In Fig. 1, a schematic of a gas turbine, HRSG and a steam turbine is represented. Mass, energy and exergy balances of the components of the system, by considering appropriate control volumes, are represented [19].

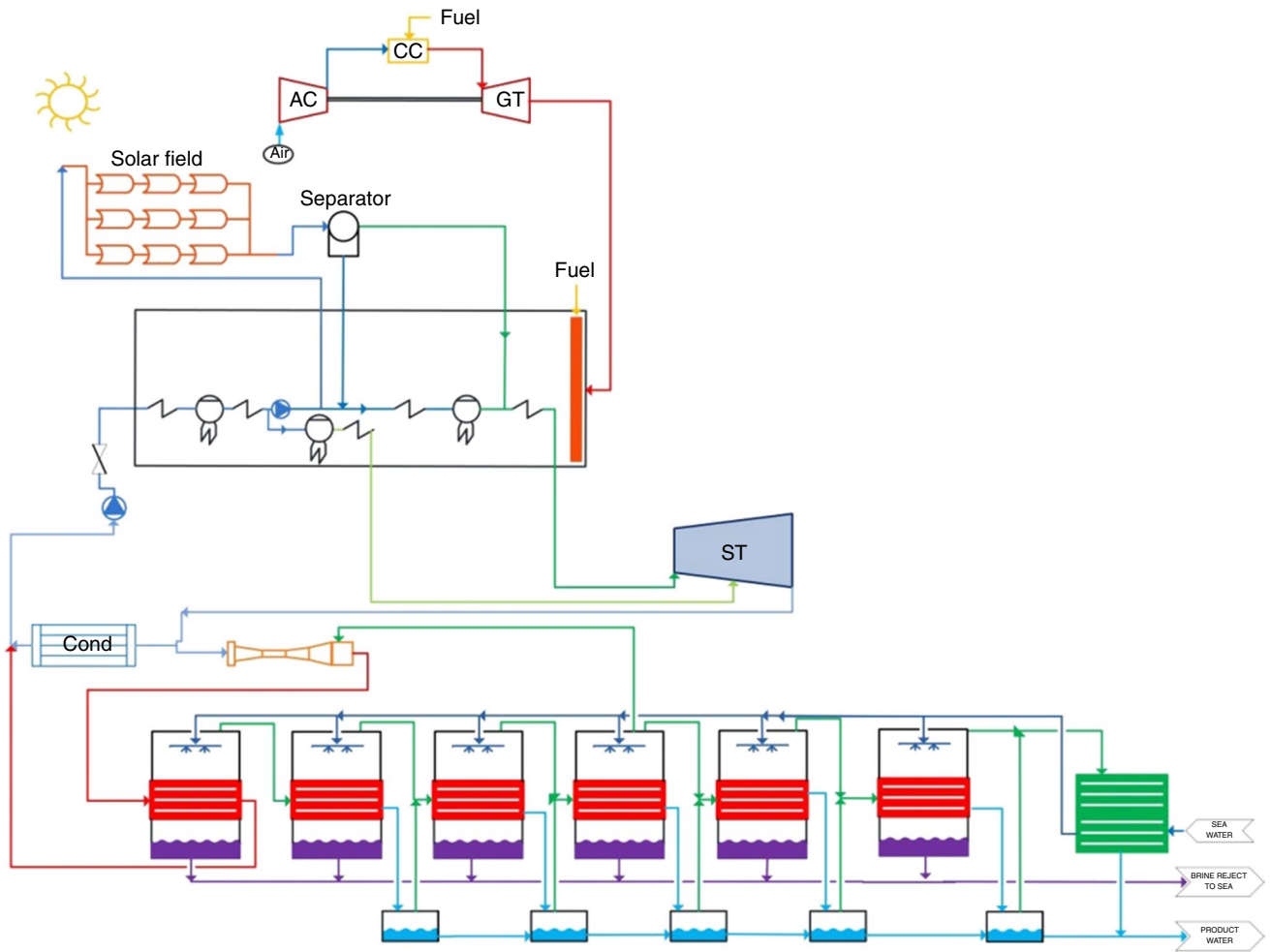
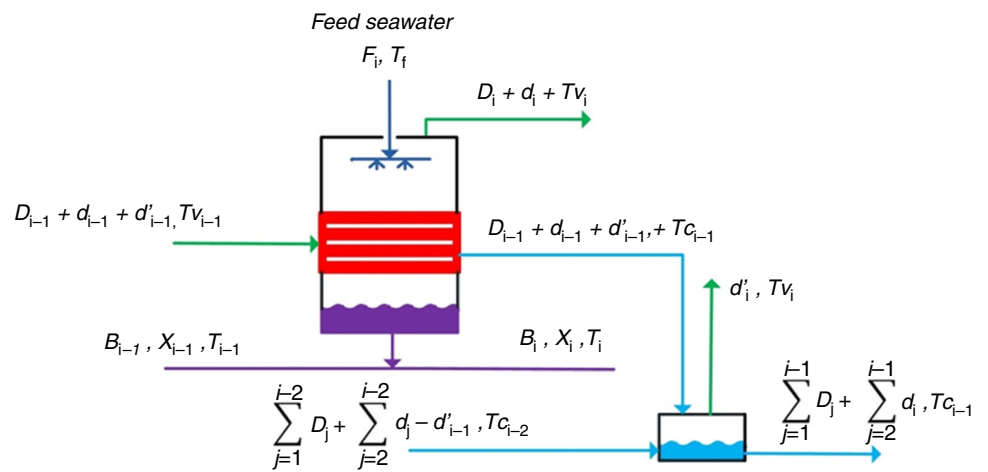


Fig. 1 The schematic of water-electricity cogeneration production power plant with solar collectors

Fig. 2 Schematic of desalination system



Desalination unit

The balanced equations of each effect are specified in Eqs. 1–8. For each effect, conservation of mass and energy are calculated [20, 21] (Fig. 2).

Water mass effect in *i*-th effect.

$$F_i + B_{i-1} = D_i + B_i \tag{1}$$

Brine mass balance in *i* effect:

$$F_i X_{F_i} + X_{B_{i-1}} B_{i-1} = X_{B_i} B_i \tag{2}$$

In relation 1 and 2, *F*, *B* and *D* show feed water, Brine water and distilled water flow rates, respectively. *F*&*B* indexes are indicators of feed water and Brine water.

The density of the Brine water released from system is as follows [20].

$$X_b = 0.9(457628.5 - 11304.11T_b + 107.5781T_b^3 - 0.360747T_b^3) \tag{3}$$

In relation 3, density of Brine water exiting the effect 4, based on ppm, is shown by *X_b* parameter.

In this relation, the maximum density for outlet water was 70,000 ppm.

The energy balance of *i*-th effect is as follows [20]:

$$D_{i-1} \lambda_{i-1} + d_{i-1} \lambda_{i-1} + d'_{i-1} \lambda'_{i-1} = F_i C_p (T_i - T_f) + D_i \lambda_i \tag{4}$$

The temperature of produced water vapor in *i*-th stage:

$$T_{vi} = T_i - \text{BPE} \tag{5}$$

In relation (5), BPE parameter is the increasing amount of water-boiling temperature due to the existence of salt in it and it is between 0.8 and 1.2. *T_{vi}* is the temperature of the steam, which is made from boiling the feed water [1].

$$T_{c,i} = T_i - \text{BPE} - \Delta T_{\text{dem}} - \Delta T_{\text{tr}} - \Delta T_c \tag{6}$$

In relation (6) *T_{c,i}* is the temperature of the steam condensed inside the next pipe effects, and it is less than the steam-boiling temperature in the previous effect. The reduction in it is due to the sum of BPE and pressure drops in humidifiers(ΔT_{dem}), friction of transfer lines(ΔT_{tr}) and drops occurred while condensation(ΔT_c).

The amount of composed steam with evaporating salt-water in effect [20]:

$$d_i = B_{i-1} C_p \frac{T_{i-1} - T'_i}{\lambda_i} \tag{7}$$

in which

$$T'_i = T_i + \text{NEA}_{\text{Brine Flash}} \tag{8}$$

In relation (8) *T_i* is the temperature in which Brine water has existed from the previous stage and enters a new stage where it will be condensed. Also, the latent heat λ_i is calculated at effect steam temperature (*T_{vi}*).

Solar collector cycle

In this power plant, a parabolic solar collector is used. Geographical features of the power plant with a parabolic solar collector is represented in Table 1.

To install the solar collectors in the north–south direction, the angle between solar radiation and normal vectors of collector plates is θ as follows [22, 23]

$$\cos \theta = \sin \varphi \sin \delta \cos \beta + \cos \varphi \cos \delta \cos \omega \cos \beta + \cos \delta \sin \omega \sin \beta \tag{9}$$

The maximum value of $\bar{I}_b \cos \theta$ is in the first days of summer. This relation achieves the received thermal power by solar collectors.

$$\dot{Q}_I = I_b A_a \cos \theta N \tag{10}$$

The absorbed thermal power by absorbers is achieved by this relation as follows [23] (Table 2).

$$\dot{Q}_a = I_b \cdot A_a \cdot \text{IAM} \cdot N \cdot \gamma_s \cdot \tau_g \cdot \alpha_a \cdot \text{IF} \cdot \eta_{\text{sd}} \cdot \text{EL} \tag{11}$$

The extractable thermal power, \dot{Q}_u , from the heat transfer fluid is calculated from the following relations [20].

$$\dot{Q}_u = F_r - (\dot{Q}_a - U_l A_r (T_i - T_e)) \tag{12}$$

$$\dot{Q}_u = m_f C_{\text{pf}} (T_e - T_i) \tag{13}$$

$$A_r = \pi D_i L \tag{14}$$

F_r as the heat loss factor of the collector is calculated from the following relation [24] (Fig. 3).

Table 1 Geographical features of water power cogeneration power plant with parabolic solar collectors

Geographical parameters of the region	Unit	Quantity
Latitude	degree	22/30
Longitude	degree	20/48

Table 2 Optical specifications of parabolic solar collectors [24]

Absorber tube outer diameter	0.7 m
Absorber tube inner diameter	0.055 m
Glass envelope outer diameter	0.115 m
Glass envelope inner diameter	0.109 m
Number of modules per collector	8
Number of collectors in a loop	8
Length of every module	12.27 m
Focal length	1.71 m
Aperture width	5.77 m
Intercept factor	0.92
Mirror reflectivity	0.92
Glass transmissivity	0.945
Solar absorptivity	0.94
Losses due to shading of heat collector element by dust on the envelope	0.98

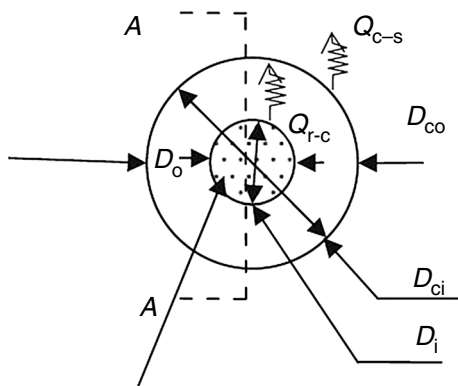


Fig. 3 Control volume of absorptive pipe of collector

$$F_r = \frac{m_f C_p}{U_L A_r} \left(1 - e^{-\left(\frac{U_L A_r F'}{m_f C_p} \right)} \right) \tag{15}$$

The heat loss factor for different values of absorbent temperature is calculated based on an iterative process and initial guess.

$$\dot{Q}_1 = \pi U_1 D_o (T_r - T_o) L \tag{16}$$

$$q_{\text{loss}} = q_{c-s} = \pi D_{co} h_w (T_{co} - T_o) + \pi \sigma D_{co} \epsilon_c (T_{co}^4 - T_{\text{sky}}^4) \tag{17}$$

$$q_{\text{loss}} = q_{c-c} = 2\pi k_c (T_{ci} - T_{co}) / \ln \left(\frac{D_{co}}{D_{ci}} \right) \tag{18}$$

$$q_{\text{loss}} = q_{r-c} = \pi D_o \sigma (T_r^4 - T_{ci}^4) / \left(\frac{1}{\epsilon_r} + \frac{D_o}{D_{ci}} \left(\frac{1}{\epsilon_c} - 1 \right) \right) \tag{19}$$

Mass, energy and exergy balance relations

Mass, energy and exergy balance relations for different components of power plant considering the proper control volume would be calculated by the following relations [25].

$$\sum_i \dot{m}_i h_i + \dot{Q} = \sum_e \dot{m}_e h_e + \dot{W} \tag{20}$$

$$\dot{E}x_Q + \sum_i \dot{m}_i ex_i = \sum_e \dot{m}_e ex_e + \dot{E}x_W + \dot{E}x_D \tag{21}$$

In order to calculate the fuel chemical exergy, the above relation could not be used; therefore, the fuel exergy is extracted through the following relation [25]

$$\xi = \frac{ex_f}{LHV_f} \tag{22}$$

For hydrocarbon gas fuels ($C_x H_y$), an experimental relation is applied for determining the value of ξ [19].

Calculating the costs of power plant investment

Thermo-economic calculations of each system are based on the investment costs of the components.

Several methods have been suggested to determine the cost of purchased equipment based on the terms of the design parameters. In this research, the cost function suggested by Rosen et al. [26] is applied; however, some corrections were done in order to have compatibility with regional conditions of Iran. To convert the investment cost rate into cost per hour, following relations should be followed:

$$\dot{Z}_k = \frac{Z_k \cdot CRF \cdot \varphi}{(h_{\text{year}} \times 3600)} \tag{23}$$

Z_k is the equipment purchasing cost based on \$. In this relation, the cost return factor (CRF) is dependent on the interest rate and the estimated life of the equipment. CRF is calculated based on the following relation [27–29]

$$CRF = \frac{ir \times (1 + ir)^n}{(1 + ir)^n - 1} \tag{24}$$

in which ir is the interest rate, and n is the total years of system operation [30].

In Eq. (23), h_{year} is the operation hours of a power plant per year, and φ is the maintenance factor which are considered 7446 and 1.06, respectively.

Cost balance equations based on SPECO methodology

To calculate the exergy cost in each flow stream, the cost balance equation is written separately for each component of the power plant. There are several thermo-economic approaches in this field. In this research, the special exergy cost method (SPECO) is used [31, 32]. This method is based on special exergy and cost of each exergy unit and auxiliary cost equations for each component of the thermal system.

Formulation of cost equation for each component of the power plant

Accordingly, the cost balance equation for a component (called *K*) in the power plant is written based on the following relation [33, 34]:

$$\sum (c_{in} \dot{E}x_{in})_k + c_{w-k} W_k = \sum (c_{out} \dot{E}x_{out})_k + c_{heat-k} \dot{E}x_{heat-k} + \dot{Z}_k \tag{25}$$

In the above relation, when a component receives work (for example in compressor or pump), the second term of the left-side expression with a positive sign is transferred to the right [32].

A collection of linear equations will be achieved by using cost balance equations and auxiliary equations of each component.

Estimating the environmental effects

Releasing CO and nitrogen oxides in the combustion chamber is due to combustion reaction. This reaction depends on different properties such as adiabatic flame temperature, which can be calculated through the following equation [4].

$$T_{pz} = A\sigma^\alpha \exp(\beta(\sigma + \lambda)^2) \pi^{x^*} \theta^{y^*} \xi^{z^*} \tag{26}$$

In this equation, θ and π refer to values of pressure and temperature, respectively. $d \xi$ shows the atomic ratio of H/C. Also, for $\Phi \leq 1$, the value of σ is equal to Φ , while for $\Phi > 1$, $\sigma = \Phi - 0.7$ is considered to determine this value. In this relation, Φ is molecular or mass ratio.

If the combustion process in the combustion chamber is assumed to be complete, the amount of CO₂ emission could be calculated by applying the following equation [17, 35]:

$$\dot{m}_{CO_2} = 44.01 \times x \times \left(\dot{m}_{fuel} / m_{fuel} \right) \tag{27}$$

x is the mole ratio of carbon in fuel and *m_{fuel}* is the molar mass of fuel. This simple equation estimates the amount of CO₂ emission in a complete combustion process.

Optimization approach

To achieve the optimum design parameters, a multi-objective optimization algorithm should be used. Although using gradient descent methods is more functional for achieving accurate optimization results, it has some defects due to its regional optimization domain and disability of being applied to discrete issues. In this research, genetic algorithm (GA) as a powerful optimization method is used.

In this research, non-dominated sorting genetic algorithm (NSGA-II) is used for optimization of CCPP variables. This algorithm applies a repetition and accidental search strategy to find an optimum value based on simple biologic principles definition of objective functions [36].

In this part, three objective functions including exergy efficiency, total products cost and CO₂ emissions are considered. In this research, the total exergy efficiency of objective function should be maximized while the two other objective functions, total products cost and CO₂ gas emission must be minimized.

CCPP exergy efficiency is shown in Eq. (28) as follows [4]:

$$\eta_{ex} = \frac{(\sum_n \dot{W}_n) + \dot{E}x_{Q_h} + \dot{E}x_{Q_c}}{\dot{E}x_f} \tag{28}$$

Equation (29) is a composed of power plant components costs, fuel cost used in combustion chamber and fire channel, and the cost related to exergy destruction.

$$\dot{C}_{Total} = \dot{C}_F + \sum_k \dot{Z}_k + \dot{C}_{Env} + \dot{C}_D \tag{29}$$

$$\dot{C}_{Env} = c_{CO_2} \dot{m}_{CO_2} \tag{30}$$

$$\dot{C}_F = c_f \dot{m}_f \times LHV \tag{31}$$

CO₂ emissions is revealed in Eq. (32), which is calculated by using the following equation [4].

$$\epsilon = \frac{\dot{m}_{CO_2}}{\dot{W}_{net} + \dot{Q}_h + \dot{Q}_c} \tag{32}$$

Decision variable and constraints

There are two independent variables in the design and optimization of the systems. Decision-making variables might be changed during optimization process, but the parameters are always constant. Other variables are dependent variables which would be calculated with the changes occurred in dependent variables based on thermodynamic relations.

In this research, 12 decision variables were selected for multi-objective optimization. Although decision variables used for optimization might be changed, these changes should occur in an acceptable range. Some of the constraints applied to thermodynamic variables in different parts of the CCPP with desalination system and solar collector are listed in Table 3.

Results and discussion

Regarding the relations described in the previous section, for each component of CCPP with desalination and solar collector and with a list of applied constraints in Table 3, multi-objective optimization was performed on design variables. Figure 4 represents the optimization results of the objective functions for the CCPP with desalination and solar collectors in the form of Pareto front.

As shown in Fig. 4, the highest exergy efficiency is at the end point of the Pareto front on the right part of the chart. At this point, the total electricity generation cost will reach its minimum value.

In multi-objective optimization, it is essential for the decision-making process to choose the final optimum solution. Decision-making process is usually done with the help of a balanced point, which is considered as an ideal state. At this point, all of the objective functions are independent of the other objective function and has its own optimum value. Simultaneous access of all three objective functions to optimum amounts is impossible. Also, the balanced point will not stay on Pareto front. The maximum point reveals exergy efficiency and minimum point represents the cost and CO₂ emission amount. The nearest point to a balanced

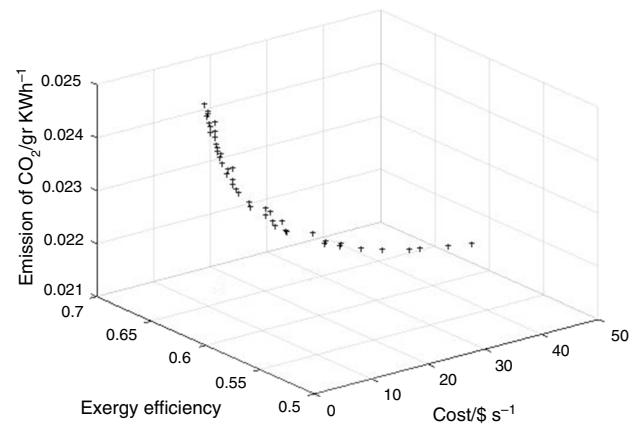


Fig. 4 Pareto front: best values for the objective functions

point in Pareto front could be considered as the final answer. However, the optimum Pareto front is weak in terms of being balanced, which means small changes in exergy efficiency, big changes occur at the generated electricity rate.

In multi-objective optimization and Pareto solution, each point could be used as the optimized point. Therefore, depending on the considered criteria of decision maker, the optimum solutions can be different. Considering the objective functions and the constraints applied to them and also applying the genetic algorithm for this purpose, the decision variables could be achieved for the combined cycle with desalination and solar collectors, whereas the final optimum point could be achieved as well.

Sensitivity analysis

The electricity generation cost and desalinated water production rate versus the variations of the number of effects and the amount of desalinated water in the CCPP are represented in Fig. 5. In Fig. 5a, as the number of effects is increased from 4 to 8, interest rate of desalinated water production will be increased; however, the exergy efficiency decreases from 52.7 to 52.4%. In Fig. 5b, as the number of effects increases from 4 to 8, the electricity generation cost will be increased from 9 to 9.4 \$ s⁻¹ and the interest rate of desalinated water generation increases from 6 to 12.

In Fig. 5c, it is shown that by increasing the number of effects, power plant emission will be decreased from 55 to 54.3 g. Also, the interest rate of desalinated water will be increased. In Fig. 5d, with an increase in the number of effects, the interest rate increases. The total exergy destruction, which is represented in different colors, will be decreased in some freshwater production tonnage and increases in other tonnages.

Table 3 The range of decision variables

Constraints	Reason
GTIT < 1550 K	Material temperature limit
$r_{AC} < 22$	Commercial availability
$\eta_{AC} < 0.9$	Commercial availability
$\eta_{GT} < 0.9$	Commercial availability
$5^{\circ}\text{C} < \text{PP}_{\text{HP}}, \text{PP}_{\text{LP}} < 30^{\circ}\text{C}$	Heat transfer limit
$5\text{bar} < P_{\text{Cond}} < 15\text{bar}$	Thermal efficiency limit
$0.75 < \eta_p < 0.9$	Commercial availability
$0.75 < \eta_{\text{ST}} < 0.9$	Commercial availability
$\dot{m}_{\text{db}} < 2\left(\frac{\text{kg}}{\text{s}}\right)$	Super heater temperature limitation
$T_{13} \geq 120^{\circ}\text{C}$	To avoid formation of sulfuric acid in exhaust gases
$P_{\text{main}} < 110\text{bar}$	Commercial availability
$3 < \text{Number of effects}(i) < 10$	Commercial availability
$3 < \text{Number of modules per collector}(N) < 10$	Commercial availability

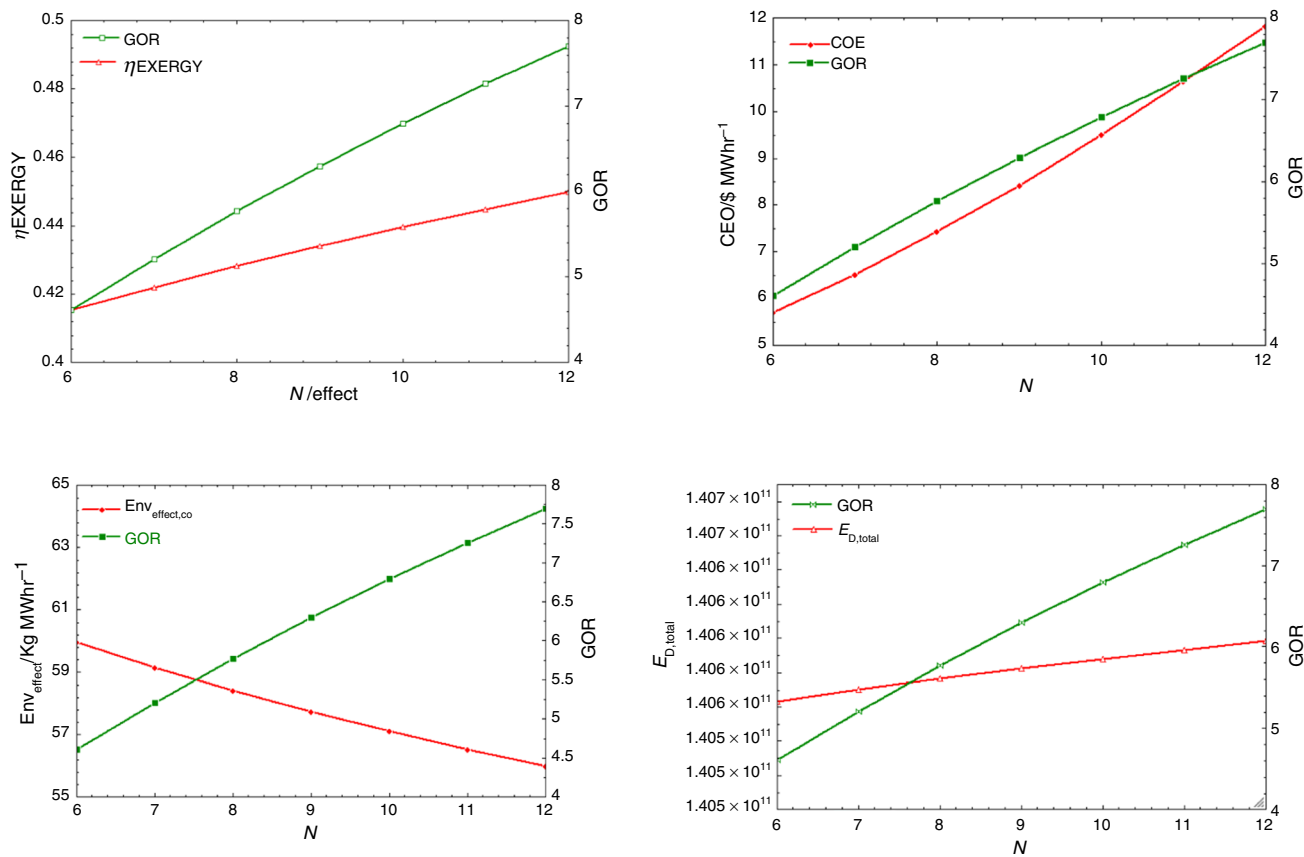


Fig. 5 Variation of number of effect and GOR with exergy efficiency, cost of electricity generation, total exergy destruction and environmental effect

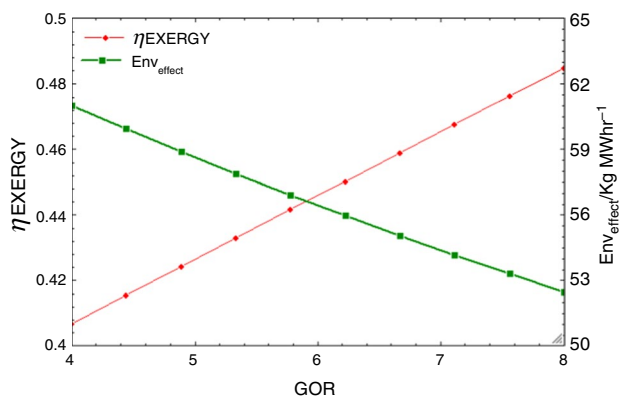


Fig. 6 The effect of GOR on exergy efficiency and environmental effect

As shown in Fig. 6, with increasing total exergy efficiency from 40 to 48%, the amount of environmental effect decreases from 61 to 52 kg MWh⁻¹. Also, by changing the

gain output ratio (GOR) from 4 to 8, the total exergy efficiency increases by 40 to 48% and the environmental effect decreases from 62 to 53 kg MWh⁻¹).

In Fig. 7, the heat received, environmental effects, the production cost and the exergy efficiency in the number of different modules that can be used for solar collectors have been analyzed. In Fig. 7a, the variation in the number of modules has a linear effect on the generation cost in power plant.

While the increase in solar energy intake did not have any effect on power plant cost, it could increase the exergy efficiency of the power plant. In Fig. 7b, variation in the number of solar power stations has a nonlinear relation with exergy efficiency changes. By increasing the heat received by the collectors, the exergy efficiency will be increased, and the environmental effects of power plant will be decreased.

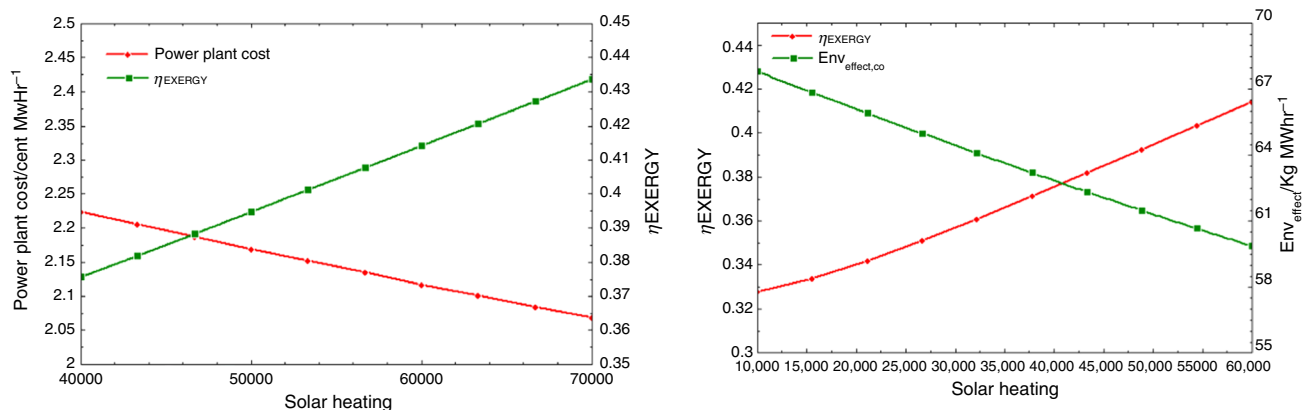


Fig. 7 Variation of exergy efficiency and solar heating with power plant cost and environmental effect

Conclusions

In the current paper, Exergoeconomic analysis base on SPECO method for a novel configuration of thermal systems including CCPP, parabolic solar collectors and multi-effect desalination was performed. The main conclusions of this research are as follows:

- Multi-objective optimization of the cogeneration system based on exergy, exergoeconomic and exergoenvironmental analysis shows that the energy efficiency of the plant is increased by 1.12%, and the exergy efficiency is increased by 1.74%.
- By increasing the number of desalination effects from 4 to 8, the rate of freshwater production increases and the exergy efficiency decreases from 52.7 to 52.4%.
- By increasing the number of effects, the cost of generating electricity increases from 9 \$ s⁻¹ to 9.4 \$ s⁻¹ and the rate of production of freshwater increases from 6 to 12.
- By increasing total exergy efficiency from 40 to 48%, the amount of environmental effect decreases from 61 to 52 kg MWh⁻¹.
- By changing the gain output ratio (GOR) from 4 to 8, the total exergy efficiency increases by 40% to 48% and the environmental effect decreases from 62 to 53 kg MWh⁻¹.

References

1. Hornburg CD, Cruver JE. Dual purpose power/water plants utilizing both distillation and reverse osmosis. *Desalination*. 1977;20:27–42.
2. El-Nashar AM, El-Baghdady A. Analysis of water desalination and power generation expansion plans for the Emirate of Abu Dhabi—a preliminary study. *Desalination*. 1984;49:271–92.
3. Kronenberg G, Lokiec F. Low-temperature distillation processes in single- and dual-purpose plants. *Desalination*. 2001;136:189–97.
4. Javadi MA, Hoseinzadeh S, Khalaji M, Ghasemiasl R. Optimization and analysis of exergy, economic, and environmental of a combined cycle power plant. *Sādhanā*. 2019;44:121.
5. Rensonnet T, Uche J, Serra L. Simulation and thermoeconomic analysis of different configurations of gas turbine (GT)-based dual-purpose power and desalination plants (DPPDP) and hybrid plants (HP). *Energy*. 2007;32:1012–23.
6. Mahbub F, Hawlader MNA, Mujumdar AS. Combined water and power plant (CWPP)—a novel desalination technology. *Desalin Water Treat*. 2009;5:172–7.
7. He WF, Zhu WP, Xia JR, Han D. A mechanical vapor compression desalination system coupled with a transcritical carbon dioxide Rankine cycle. *Desalination*. 2018;425:1–11.
8. Ramezanizadeh M, Alhuyi Nazari M, Ahmadi MH, Açıklalp E. Application of nanofluids in thermosyphons: a review. *J Mol Liq*. 2018;272:395–402.
9. Habibollahzade A, Gholamian E, Ahmadi P, Behzadi A. Multi-criteria optimization of an integrated energy system with thermoelectric generator, parabolic trough solar collector and electrolysis for hydrogen production. *Int J Hydrogen Energy*. 2018;43:14140–57.
10. Sadi M, Arabkoohsar A. Exergoeconomic analysis of a combined solar-waste driven power plant. *Renew Energy*. 2019;141:883–93.
11. Wang J, Lu Z, Li M, Lior N, Li W. Energy, exergy, exergoeconomic and environmental (4E) analysis of a distributed generation solar-assisted CCHP (combined cooling, heating and power) gas turbine system. *Energy*. 2019;175:1246–58.
12. Ortega-Delgado B, Cornali M, Palenzuela P, Alarcón-Padilla DC. Operational analysis of the coupling between a multi-effect distillation unit with thermal vapor compression and a Rankine cycle power block using variable nozzle thermocompressors. *Appl Energy*. 2017;204:690–701.
13. Sharan P, Neises T, McTigue JD, Turchi C. Cogeneration using multi-effect distillation and a solar-powered supercritical carbon dioxide Brayton cycle. *Desalination*. 2019;459:20–33.
14. Yilmaz F. Thermodynamic performance evaluation of a novel solar energy based multigeneration system. *Appl Therm Eng*. 2018;143:429–37.
15. Ghorbani B, Mahyari KB, Mehrpooya M, Hamed M-H. Introducing a hybrid renewable energy system for production of power and fresh water using parabolic trough solar collectors and LNG cold energy recovery. *Renew Energy*. 2020;148:1227–43.
16. Demir ME, Dincer I. Development of an integrated hybrid solar thermal power system with thermoelectric generator for desalination and power production. *Desalination*. 2017;404:59–71.
17. Ansari M, Beitollahi A, Ahmadi P, Rezaie B. A sustainable exergy model for energy–water nexus in the hot regions: integrated

- combined heat, power and water desalination systems. *J Therm Anal Calorim.* 2020. <https://doi.org/10.1007/s10973-020-09977-1>.
18. Al-Mutaz IS, Wazeer I. Development of a steady-state mathematical model for MEE-TVC desalination plants. *Desalination.* 2014;351:9–18.
 19. Javadi MA, Hoseinzadeh S, Ghasemiasl R, Heyns PS, Chamkha AJ. Sensitivity analysis of combined cycle parameters on exergy, economic, and environmental of a power plant. *J Therm Anal Calorim.* 2020;139:519–25.
 20. Javadi MA, Khalaji M, Ghasemiasl R. Exergoeconomic and environmental analysis of a combined power and water desalination plant with parabolic solar collector. *Desalin Water Treat.* 2020;193:212–23.
 21. Hoseinzadeh S, Ghasemiasl R, Javadi MA, Heyns PS. Performance evaluation and economic assessment of a gas power plant with solar and desalination integrated systems. *Desalin Water Treat.* 2020;174:11–25.
 22. Ozgener O, Hepbasli A. Exergoeconomic analysis of a solar assisted ground-source heat pump greenhouse heating system. *Appl Therm Eng.* 2005;25:1459–71.
 23. Javadi MA, Ahmadi MH, Khalaji M. Exergetic, economic, and environmental analyses of combined cooling and power plants with parabolic solar collector. *Environ Prog Sustain Energy.* 2019;39:e13322.
 24. Adibhatla S, Kaushik SC. Energy, exergy and economic (3E) analysis of integrated solar direct steam generation combined cycle power plant. *Sustain Energy Technol Assess.* 2017;20:88–97.
 25. Bejan A, Tsatsaronis G, Moran MJ. *Thermal design and optimization.* Hoboken: Wiley; 1995.
 26. Rosen MA, Dincer I. Thermo-economic analysis of power plants: an application to a coal fired electrical generating station. *Energy Convers Manag.* 2003;44:2743–61.
 27. Hammond GP, Ondo Akwe SS. Thermodynamic and related analysis of natural gas combined cycle power plants with and without carbon sequestration. *Int J Energy Res.* 2007;31:1180–201.
 28. Jin Z-L, Dong Q-W, Liu M-S. Exergoeconomic analysis of heat exchanger networks for optimum minimum approach temperature. *Huaxue Gongcheng (Chem Eng).* 2007;35:11–4.
 29. Oktay Z, Dincer I. Exergoeconomic analysis of the Gonen geothermal district heating system for buildings. *Energy Build.* 2009;41:154–63.
 30. Kanoglu M, Dincer I, Rosen MA. Understanding energy and exergy efficiencies for improved energy management in power plants. *Energy Policy.* 2007;35:3967–78.
 31. Rosen MA, Dincer I. Effect of varying dead-state properties on energy and exergy analyses of thermal systems. *Int J Therm Sci.* 2004;43:121–33.
 32. Lozano MA, Valero A. Theory of the exergetic cost. *Energy.* 1993;18:939–60.
 33. Orhan MF, Dincer I, Rosen MA. Exergoeconomic analysis of a thermochemical copper–chlorine cycle for hydrogen production using specific exergy cost (SPECOC) method. *Thermochim Acta.* 2010;497:60–6.
 34. Rovira A, Sánchez C, Muñoz M, Valdés M, Durán MD. Thermo-economic optimisation of heat recovery steam generators of combined cycle gas turbine power plants considering off-design operation. *Energy Convers Manag.* 2011;52:1840–9.
 35. Akbari Wakilabadi M, Bidi M, Najafi AF, Ahmadi MH. Energy, Exergy analysis and performance evaluation of a vacuum evaporator for solar thermal power plant Zero Liquid Discharge Systems. *J Therm Anal Calorim.* 2020;139:1275–90.
 36. Ahmadi P, Dincer I. Exergoenvironmental analysis and optimization of a cogeneration plant system using Multimodal Genetic Algorithm (MGA). *Energy.* 2010;35:5161–72.

Publisher's Note Springer Nature remains neutral with regard to jurisdictional claims in published maps and institutional affiliations.